Gondwana Research 125 (2024) 378–389

Contents lists available at ScienceDirect

Gondwana Research

journal homepage: www.elsevier.com/locate/gr

Continental climate variability during the middle Eocene global warming

Yu Han [a], Yingchang Cao [a,b], Chao Liang [a,b,*], Keyu Liu [a,b,c], Fang Hao [a,b]

[a] School of Geosciences, China University of Petroleum (East China), Qingdao, Shandong 266580, China
[b] Laboratory for Marine Mineral Resources, Qingdao National Laboratory for Marine Science and Technology, Qingdao, Shandong 266071, China
[c] CSIRO Energy, Kensington, Western Australia, Australia

ARTICLE INFO

Article history:
Received 29 November 2022
Revised 8 May 2023
Accepted 14 August 2023
Available online 19 September 2023
Handling Editor: Richard Palin

Keywords:
East Asia
Terrestrial shale
Astronomical forcing
Paleoclimate transition
Middle Eocene

ABSTRACT

Middle Eocene saw several global warming events. However, the terrestrial climate linkage to the warming events is still enigmatic. Particularly, the paleoclimate of middle Eocene East Asia is unclear when the East Asian monsoons started to prevail. Here, we present a combination of high-resolution elemental, compositional and natural gamma-ray (GR) records and conduct an orbital-scale paleoclimate reconstruction for the middle Eocene lacustrine shale dated from 43.4 to 40.9 Ma in the Bohai Bay Basin, East Asia. The results show an obvious shift in orbital variability from obliquity- to eccentricity-dominated cycles and an evident humidification at ~41.9 Ma in the East Asia. Eccentricity maxima filtered from the terrestrial records coincide with the deep-sea temperature rises during ~41.9–41.5 Ma. The terrestrial climate transition at 41.9 Ma was most likely attributed to intensification of the East Asian monsoons responding to the elevated atmospheric pCO_2 during the concurrent global warming.

1. Introduction

Eocene (~56 to 33.9 Ma) is the latest greenhouse stage in the Earth history, characterized by substantially higher temperature and atmospheric pCO_2 than the present (Anagnostou et al., 2016; Greenwood and Wing, 1995) and it could be an analogy of our global warming future (Lunt et al., 2013; Ma et al., 2019). A series of global warming events occurred prior to the onset of the icehouse state at the Eocene-Oligocene boundary of ~34 Ma (Barrett, 2003; Zachos et al., 2008), including the Paleocene/Eocene Thermal Maximum (PETM), the Middle Eocene Climatic Optimum (MECO), and the recently defined Late Lutetian Thermal Maximum (LLTM, or called the chron C19r event) (Bosboom et al., 2014b; Giorgioni et al., 2019; Intxauspe-Zubiaurre et al., 2018; Rivero-Cuesta et al., 2020; Westerhold and Röhl, 2013; Westerhold et al., 2018; Zachos et al., 2010). The climate pattern of East Asia during middle Eocene is still under debate (Licht et al., 2014; Ma et al., 2019; Zhang et al., 2012). Based on palynofloral assemblages, fossil plants and lithological records, the Paleogene climate in China is divided into three latitudinal zones: a humid warm temperate to subtropical zone in the north controlled by the westerlies, an arid zone in the middle controlled by the subtropical high pressures, and a humid tropical to subtropical zone in the south (Song et al., 1983; Sun and Wang, 2005; Wu et al., 2018) (Fig. 1A). It was suggested that the planetary wind dominated climate system in East Asia shifted to the modern monsoon dominated climate system at around 25–22 Ma (Guo et al., 2008; Sun and Wang, 2005), when the aeolian dust of the Chinese Loess Plateau carried by the winter monsoons started to deposit (Guo et al., 2002; Qiang et al., 2010). However, studies have reported the existence of early stage East Asian monsoons during the Eocene (Licht et al., 2014; Quan et al., 2011; Quan et al., 2012), which was linked to the uplift of the Tibetan-Himalayan orogen (Dupont-Nivet et al., 2008; Molnar et al., 2010), the retreat of the Paratethys Sea (Bosboom et al., 2011; Carrapa et al., 2015), and the increase of atmospheric pCO_2 (Licht et al., 2014). Thus, the details of climate variations in Eocene East Asia are still unclear.

Orbital forcing plays an important role in regulating paleoclimate changes both in marine and lacustrine paleoenvironments (Meyers, 2015, 2019; Li et al., 2018; Westerhold et al., 2020; Jin et al., 2022). Under different climatic backgrounds, the orbit forcing of paleoclimate has different characteristics: Westerhold and Röhl (2013) found that the ocean temperature was paced by eccentricity during the Eocene greenhouse stage, and obliquity signal was then amplified by the initial ice sheet at high latitudes during the cooling trend afterwards (Westerhold and Röhl, 2009); The sapropels in the middle-latitude Mediterranean Sea is reported to form when the Nile runoff is raised by intensified African summer

* Corresponding author at: School of Geosciences, China University of Petroleum (East China), Qingdao, Shandong 266580, China.
E-mail address: liangchao0318@163.com (C. Liang).

https://doi.org/10.1016/j.gr.2023.08.020
1342-937X/

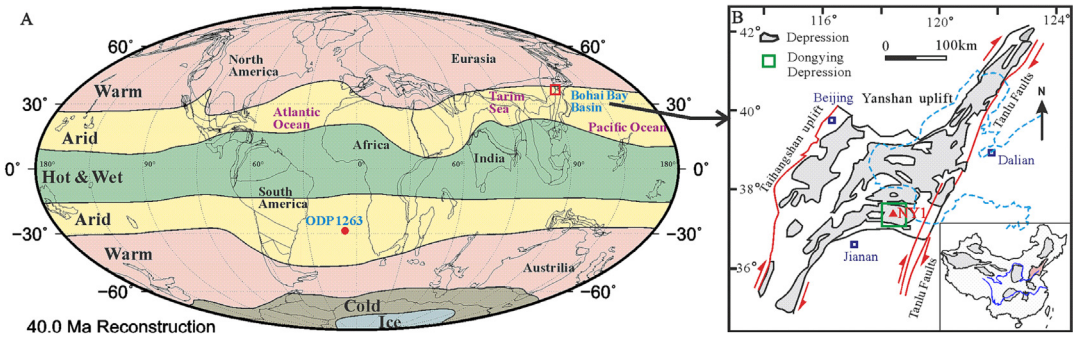

Fig. 1. Paleogeography and location map of the study site. (A) 40 Ma Paleogeography reconstruction in Mollweide projection (from http://www.odsn.de) indicating the location of the Bohai Bay Basin, ODP site 1263 and zonal climate distributions (modified from Scotese (Scotese, 2016), Jin et al. (2022). (B) Structural map of the Bohai Bay Basin and the location of the well NY1 in the Dongying Depression.

monsoon which is paced by precession (Rohling et al., 2015). The paleoclimate transition and variability could be captured by the shifts in astronomical signals recorded in sediments. One typical case is the mid-Pleistocene transition (MPT): in the high-latitude marine realm, the paleoclimate periodicity shifted from obliquity cycles to short eccentricity cycles during the MPT; while in the monsoon-induced middle-latitude East Asia, a dominant precession periodicity was replaced by combined 100, 41, and 23-kyr cycles after the MPT (Pisias and Moore, 1981; Raymo et al., 2006; Sun et al., 2019). However, the reason for this kind of orbital forcing variability still needs further researching.

Fine-grained lacustrine sedimentary rocks are excellent carriers of terrestrial climate information and good records to investigate the orbital forcing of climates (Aswasereelert et al., 2013; Hinnov, 2018; Shi et al., 2019; Wu et al., 2014). The lower third member (Es3l) to the upper fourth member (Es4u) of the Shahejie Formation contains a thick (175 m) succession of laminated shale in the Bohai Bay Basin in Eastern China (Fig. 2). In the middle Eocene zonal climate pattern, the study area was close to the boundary of the arid zone controlled by the subtropical high and the humid zone controlled by the westerlies, and was close to the vapor source of summer monsoons from the Pacific Ocean (Fig. 1A). Therefore the study site is sensitive to the hydroclimate oscillations. Although a number of cyclostratigraphy and magnetic stratigraphy researches have been conducted in Eocene Bohai Bay Basin with astronomical time scale established (Chen et al., 2020; Jin et al., 2022; Shi et al., 2019; Zhao et al., 2019), the orbital forced paleoclimate variability and its link to the global climate are yet to be explored in detail.

Here, we present a combination of elemental, compositional and natural gamma-ray (GR) records for the middle Eocene (middle Lutetian to lower Bartonian) lacustrine shale from the well NY1 (~43.4–41 Ma) in the Dongying Depression of the Bohai Bay Basin. Paleoclimate reconstruction and cyclostratigraphy analysis were conducted to investigate the orbital forcing of the shale deposition and terrestrial climate during the Eocene greenhouse world.

2. Geological background

The Bohai Bay Basin is a Mesozoic-Cenozoic fault depression basin located at eastern China with a latitude range of 35° N–40° N. Dongying Depression is located in the southern Bohai Bay Basin (Fig. 1) and filled with Paleozoic, Mesozoic, and Cenozoic strata from bottom to top. The Cenozoic strata further consist of Paleogene, Neogene, and Quaternary rocks (Fig. 2). Among these, the thick Paleogene strata is composed of the Kongdian (Ek), Shahejie (Es), and Dongying (Ed) formations (Liang et al., 2017). The Shahejie Formation is further divided into four members: the Es4, Es3, Es2, and Es1 and the black shale from the lower third member (Es3l) to the upper fourth member (Es4u) is the study interval of this research. During the sedimentation period of Es4u and Es3l shale, the Bohai Bay Basin was in an intense rifting and expansion stage and the Dongying Depression developed a high-salinity semi-deep lake environment (Liang et al., 2017; Zahid et al., 2016). The anoxia condition at the lake bottom and high salinity favored the formation and preservation of up to 200 m black shale in the Dongying Depression of the Bohai Bay Basin (Li et al., 2018).

The coring well NY1 is drilled by Sinopec for the evaluation of shale oil potential; the depth of the well NY1 is from 3498 m to 3295 m with a drilling length of 203 m and a coring length of 185.22 m (recovery rate: 91%). The core was cut open after being drilled, and one third of the core was preserved for long term observation and the rest of the core was accessed for sampling. The well NY1 was sited close to the deposition center of the Dongying Depression and preserved a good sedimentary record of lacustrine shale of Es3u to Es3l formations.

A number of cyclostratigraphy researches have been conducted in Eocene Bohai Bay Basin, but the establishment of the astronomical time scale was hampered due to the lack of absolute age. Shi et al. (Shi et al., 2019) conducted a high resolution magnetic stratigraphy for the Shahejie Formation in the Dongying Depression and set the boundary of Es3l and Es4u to be 41.38 Ma, which provided a precise time constrain in the study area.

3. Data and methods

3.1. Rock characteristics analysis

The samples for this study come from 175-m-thick core of the well NY1 in the Dongying Depression of the Bohai Bay Basin (Fig. 1A). Mineralogical features and compositional variations of the samples were investigated through a series of methods including thin sections observations of 196 samples, X-ray diffraction (XRD) analysis of 665 samples that were collected at a ~0.2 m interval, elemental concentration analysis of 98 samples and TOC analysis of 170 samples. Thin sections were prepared to be as thin as 0.03 mm and a polarizing Zeiss microscope was used for the thin section observations. XRD analyses were conducted using a D/max 2500 TTR at the Petroleum Geology Research Center of the Geological Sciences Institute of the Shengli Oilfield, Sinopec; before analyzing, each sample was dried at 40 °C for 2 days and grounded by an agate mortar to a size less than 40 mm. Then computer diffractogram analysis was performed to identify and calculate the relative abundances (wt %) of the minerals. TOC content was obtained by a CS344 carbon sulfur detector (Leco Company, US) which has an absolute deviation less than or equal to 0.01 mg/g. The concentrations of elements Mg, Ca, Na, Al and K

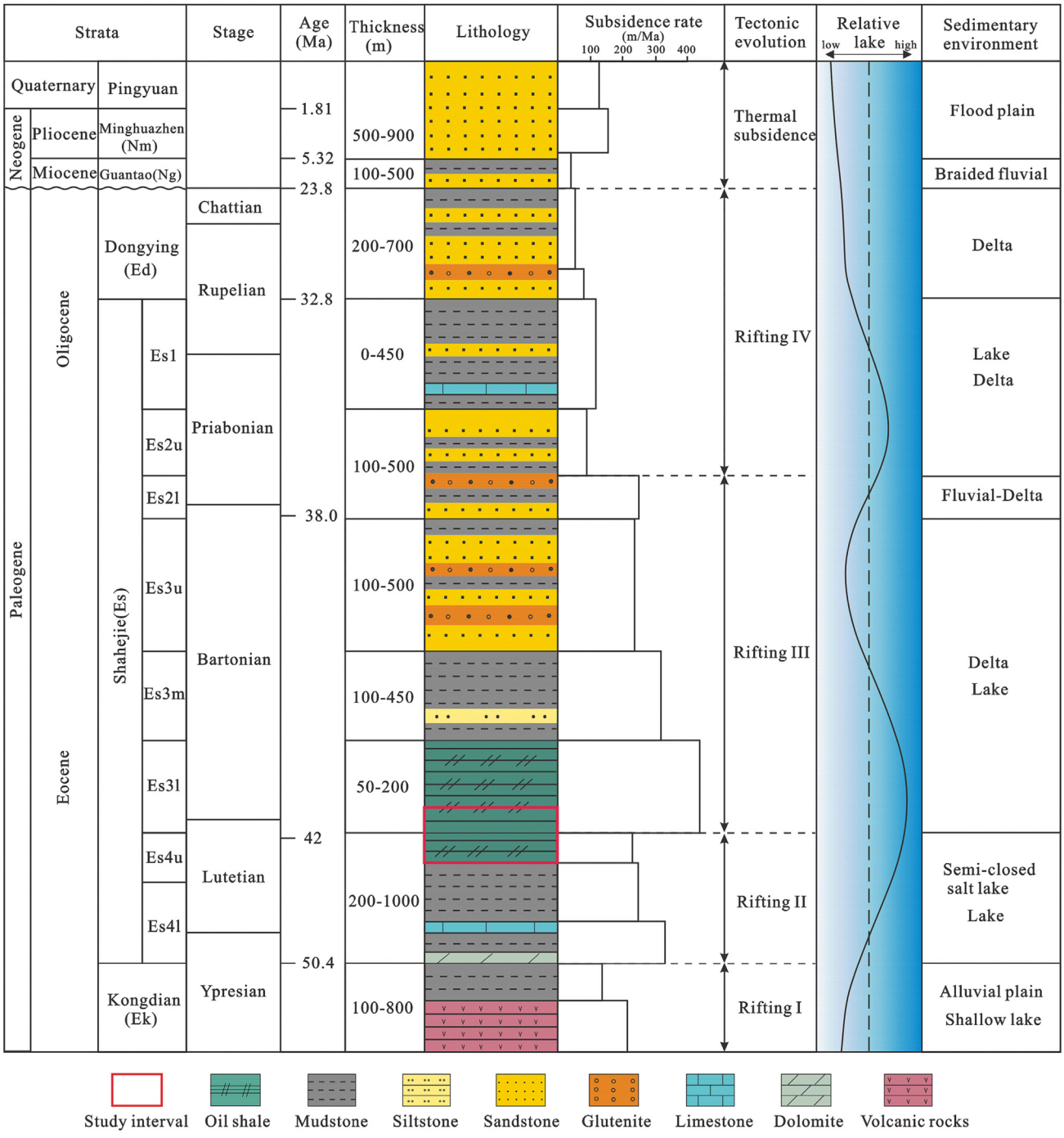

Fig. 2. Stratigraphic column of the Bohai Bay Basin, modified from Liang et al. (2017) and He et al. (2017).

were determined using an inductively coupled plasma-atomic emission spectrometer (ICP-AES, JY38S) at the Shengli Oilfield, Sinopec. Samples were ground to 200-mesh and all experiments were performed under an ambient temperature of 70–75 °C and a relative humidity less than 70%. In this study the dolomite content, Mg/Ca ratios, Na/Al ratios and the chemical index of alternation were used as proxies for the paleoclimate.

3.2. Natural gamma-ray logging

The natural gamma-ray (GR) data were collected at a sampling rate of 0.038 m and provided by the Shengli Oilfield Company of SINOPEC. The content variation of potassium (K), uranium (U), thorium (Th) and their daughter elements could be reflected by GR data, and these elements are preferentially enriched in clay minerals, K-feldspar and organic matter (Schnyder et al., 2006). GR logging has been widely used as a paleoclimate proxy in cyclostratigraphy analyses as it has a high signal-to-noise ratio and stability (Li et al., 2019; Huang et al., 2023). Zhang et al. (2022a) found lime mudstones coincide with low GR values while mudstones coincide with high GR values in the Shahejie Formation of Bohai Bay Basin. Studies also showed that high GR values could be correlated to warm and humid paleoclimate with high eccentricity in Bohai Bay Basin and Songliao Basin (Jin et al., 2022;

Wu et al., 2014). Therefore, the GR series of well NY1 (available in Supplementary file) were adopted as the climate proxy for cyclostratigraphy analysis in this study.

3.3. Time series analysis

The natural gamma-ray (GR) records of the well NY1 was used for time series analysis via the Acycle v2.6 software (Li et al., 2019). Before analyzing, the GR logging series were firstly preprocessed through interpolation and detrending. Sub-section Ⅰ and Ⅱ were LOWESS detrended using window sizes of 47.8 m and 57 m separately. Then the 2π-Multi-Taper method (MTM) was performed to analyze the power spectra in order to identify the astronomical signals in the preprocessed data and Evolutionary Fast Fourier Transform (Evolutionary-FFT) method was used to characterize continuous signal variations in frequencies. A window of 59.9 m and a step of 0.48 m were applied in the Evolutionary-FFT process. A 20% median smoothed window was used for the robust red noise models. The peaks in the power spectra with confidence level over 95% were analyzed and then filtered through Gaussian bandpass filtering to isolate eccentricity (0.033663 ± 0.006), obliquity (0.33 224 ± 0.016) and precession (0.56642 ± 0.04) cycles in sub-section Ⅰ, and eccentricity (0.033738 ± 0.008), obliquity (0.36192 ± 0.038) and precession (0.47479 ± 0.02) cycles in sub-section Ⅱ.

Several researchers have conducted detailed cyclostratigraphy studies on the well FY1 in the study area and their results showed that the bottommost long eccentricity cycle of Es3l could be correlated to the 102th long eccentricity cycle (E102) of the theoretical astronomical solution (Shi et al., 2019; Jin et al., 2022; Ma et al., 2023; Laskar et al., 2011). In addition, bed-to-bed correlation between well NY1 and FY1 was achieved by peak-to-peak matching of GR values which revealed a high strata comparability between the two wells (Zhang et al., 2022a). Therefore we filtered the 405 kyr component from the GR series and anchored the bottommost 405kyr cycle of Es3l to the E102 of the Laskar2010d solution. A cycle-by-cycle correlation was obtained and a time framework of the well NY1 was built. As for the phase relation, high 405-kyr GR peaks associated with humid climates were tuned to long (405-kyr) eccentricity maxima. Furtherly, correlation coefficient (COCO) analysis was performed in order to recognize the most optimal sedimentation rates of the study interval. Previous studies showed that the sedimentary rates of the Shahejie Formation in the Dongying Depression were 8–12 cm/kyr through magnetostratigraphy and cyclostratigraphy analyses (Shi et al., 2019; Jin et al., 2022; Ma et al., 2023), therefore the test sedimentary rate ranges were set to be 5–20 cm/kyr. The null hypothesis (H0) significance level of no astronomical forcing was calculated through 2000 times Monte Carlo simulations. The evolutionary correlation coefficient (eCOCO) method was also applied to track the sedimentation rate variations with a sliding window of 50 m and a step of 0.038 m. The middle age of the target astronomical solution is set to be 42.5 Ma.

4. Results

4.1. Mineralogy analysis

The 175-m-thick interval is divided into two sub-sections given the evident differences in petrology, mineral compositions, paleoclimate records and orbital forcing (Fig. 3). X-ray diffraction (XRD) analysis of 665 samples was conducted in this study to find that calcite is the most abundant mineral in the middle Eocene lacustrine shale in Bohai Bay Basin with an average of 38.9% (Fig. 3b). Quartz has an average content of 22.9%, followed by clay minerals (average: 21.1%), dolomite (average: 9.8%), feldspar (average: 3.8%) and pyrite (average: 2.8%). The clay content is inversely proportional to the calcite content. The sub-section Ⅰ has a higher dolomite content (average: 12.8%) than the sub-section Ⅱ (average: 5.4%) (Fig. 3i), and has a lower calcite content (average: 36.4%) than the sub-section Ⅱ (average: 42.7%). Besides, 170 TOC samples of the study interval show a range between 0.58% and 12.8% with an average of 3.16% (Fig. 3c).

Laminated structures are common in the Paleogene shale of the Bohai Bay Basin, which are represented by alternation of light carbonate laminae (calcite or dolomite) and dark silt–clay and organic matter laminae. The thickness of the light carbonate lamina is about 100–250 μm and it usually has an abrupt bottom boundary with the underlying dark lamina. Algal filaments can be vaguely recognized. The dark silt–clay and organic lamina is usually 40–100 μm thick and sometimes extremely thin organic matter laminae (less than 10 μm thin) can be seen at the bottom of clay laminae. Based on mineral compositions, sedimentary structures and TOC content, four lithofacies can be identified for the shale of the study interval: high-TOC calcareous shale, low-TOC calcareous shale, high-TOC dolomitic shale and low-TOC anhydrite. The high-TOC calcareous shale is dark grey in color, rich in calcite, clay minerals and quartz, and has well-developed laminae (Fig. 4A). In contrast to the high-TOC calcareous shale, the low-TOC calcareous shale is light grey and has blurry laminae boundaries (Fig. 4B). The high-TOC dolomitic shale is grey-black in color, rich in dolomite, clay minerals and quartz, and has clearer laminae boundaries (Fig. 4C). The low-TOC anhydrite is featured by euhedral anhydrite and TOC lower than 2% (Fig. 4D). High-TOC calcareous shale and low-TOC calcareous shale are the dominant lithofacies in the sub-section Ⅱ, while high-TOC dolomitic shale interbedded with high-TOC calcareous shale are dominant in the sub-section Ⅰ. The Low-TOC anhydrite exist at the bottom of Es4u of the Shahejie Formation.

4.2. Time series analysis

Time series analysis has been conducted on the GR series which ranges from 42 to 108 API with an average of 75 API in the study interval (Fig. 3k). Evolutionary power spectra analysis of the preprocessed and detrended GR series show a significant orbital variability from sub-section Ⅰ to sub-section Ⅱ. The sub-section Ⅰ displays a dominated 3 m cycles while the sub-section Ⅱ is dominated by a much larger 37 m cycles (Fig. 3m).

Evolutionary correlation coefficient analysis of the study interval suggest that shale of sub-section Ⅰ has a sedimentation rate of ~6.1 cm/kyr which quickly increases to 9–10 cm/kyr in sub-section Ⅱ, together with the results of the evolutionary analysis of the null hypothesis (H_0) significance level without astronomical forcing (Fig. 3n, o). Eccentricity, obliquity and precession cycles are identified through the power spectra analyses of sub-section Ⅰ and sub-section Ⅱ GR series separately using the 2π-Multi-Taper Method (MTM) (Fig. 5). However, the sub-section Ⅰ shale is dominated by the 40 kyr obliquity cycles whereas the sub-section Ⅱ shale is dominated by the 405 kyr eccentricity cycles. Previous magnetic stratigraphy and cyclostratigraphy research in the study area and the well-preserved Milankovitch cycles in this study enable us to tune the GR series to the astronomical solution in the time domain using the 405 kyr filter (Fig. 6). The boundary of sub-section Ⅰ and sub-section Ⅱ is ~41.9 Ma.

4.3. Paleoclimate records

Sodium ions are easier to be enriched in the sediments in dry climate when chemical weathering is weak, whereas aluminium ions are the opposite. Thus a high Na/Al ratio indicates a dry climate (Sawyer, 1986). The process of Mg^{2+} replacing Ca^{2+} in

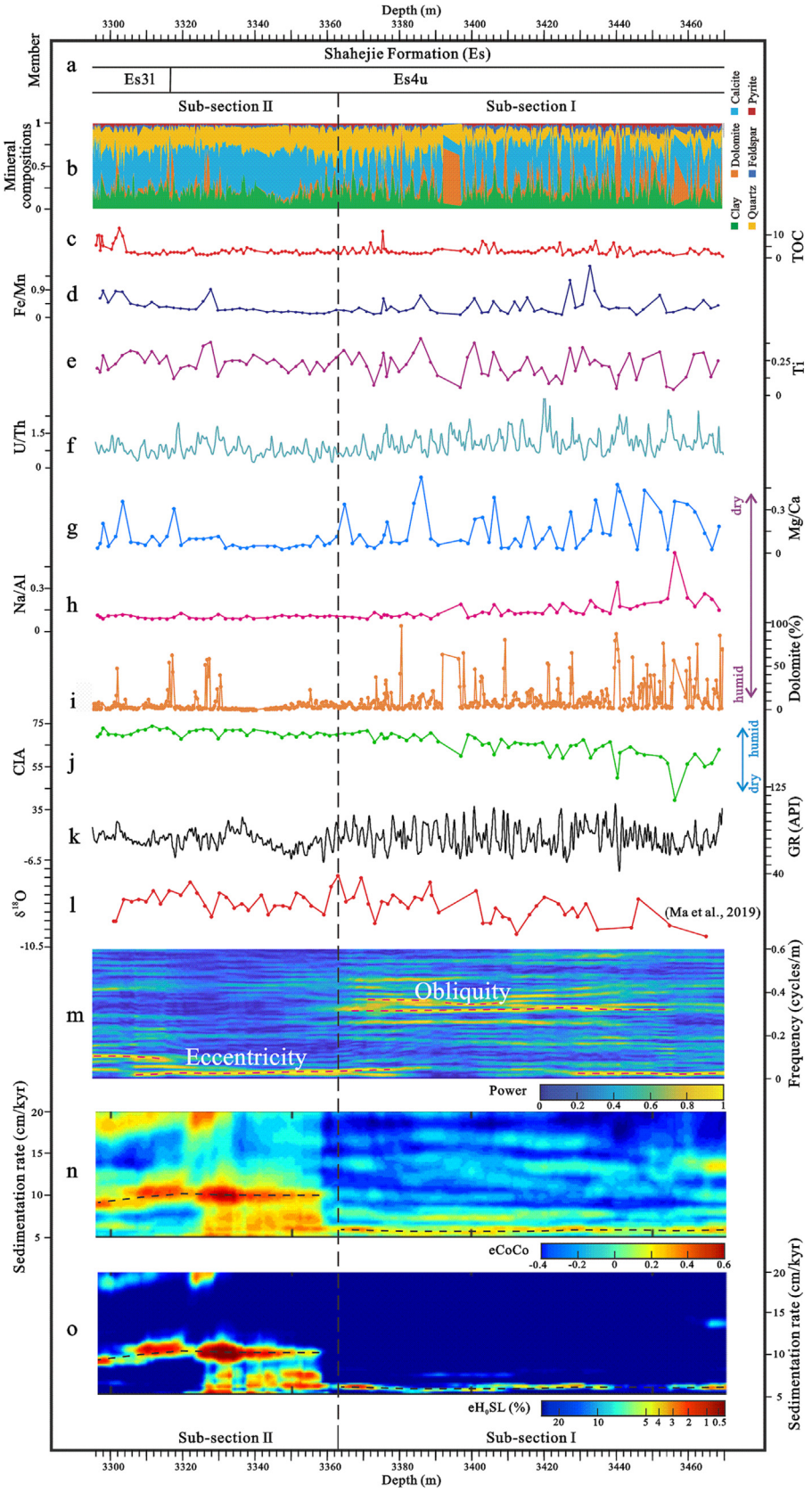

Fig. 3. Paleoclimate and cyclostratigraphy records of the well NY1 in the Bohai Bay Basin. a Members of the Shahejie Formation. b Mineral compositions. c TOC content. d, e, f, g, h Fe/Mn, Ti, U/Th, Mg/Ca, Na/Al records. i Dolomite content. j CIA records. k GR records. l Bulk carbonate $\delta^{18}O$ of the well NY1(Ma et al., 2019). m Evolutionary power spectra using fast Fourier transform method. n Sedimentation rate analysis using eCOCO method. o Evolutionary H_0 significance level of no astronomical forcing.

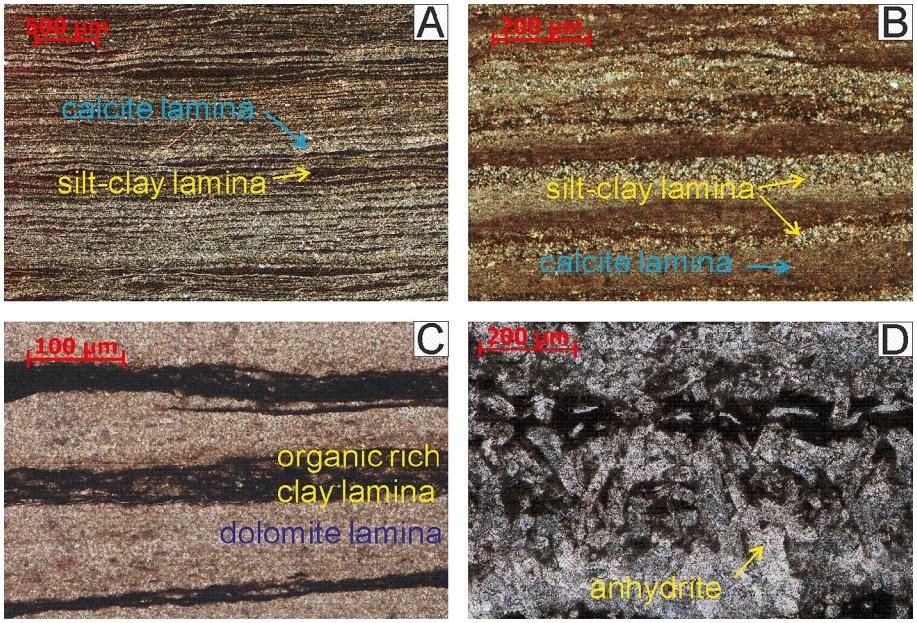

Fig. 4. Microscopic characteristics of the Shahejie Formation shale, well NY1. (A) High-TOC calcareous shale under plane-polarized light (sub-section Ⅱ of well NY1, 3318 m). (B) Low-TOC calcareous shale under plane-polarized light (sub-section Ⅱ of well NY1, 3316.3 m). (C) High-TOC dolomitic shale under plane-polarized light (sub-section Ⅰ of well NY1, 3466.15 m). (D) Low-TOC anhydrite under plane-polarized light (sub-section Ⅰ of well NY1, 3488.56 m).

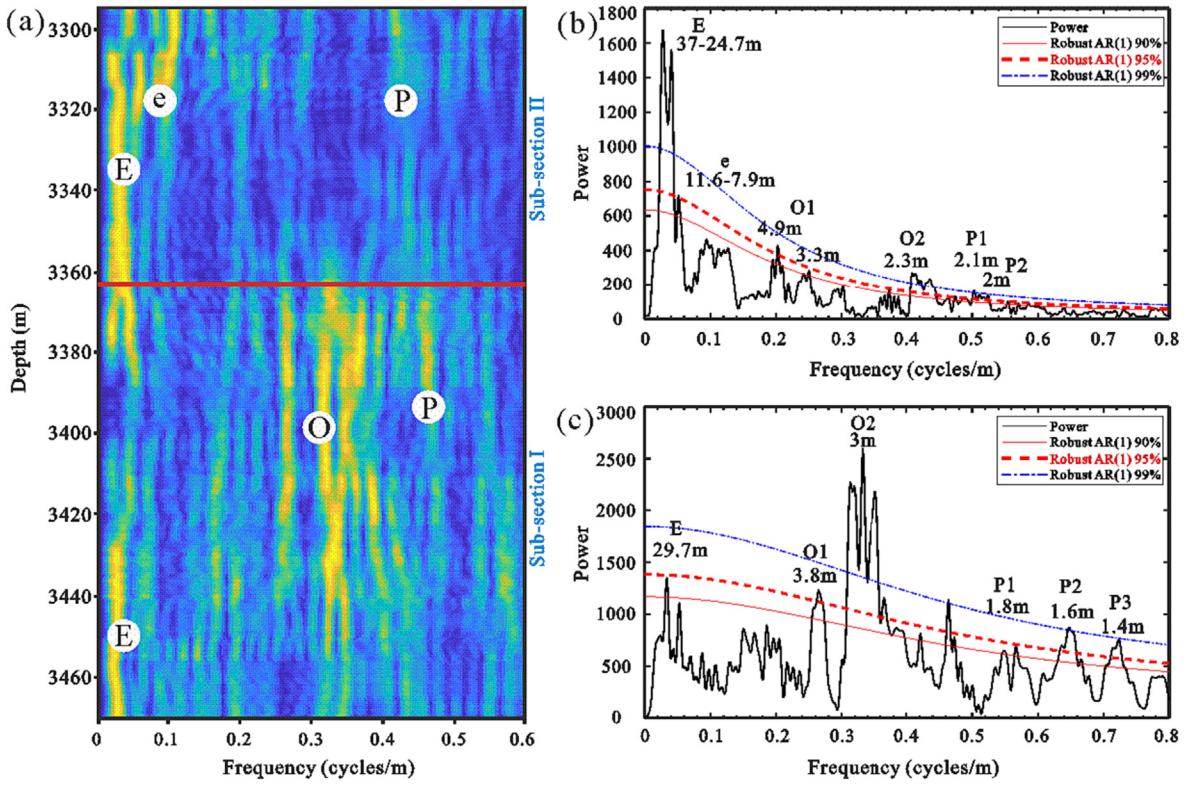

Fig. 5. Spectral analysis of the study interval's GR series. a Evolutionary power spectrum analysis of the GR series and FFT spectrogram with a 59.9108 m sliding window. The red line indicates the boundary of sub-section Ⅰ and Ⅱ. **b** 2π-Multi-taper method (MTM) power spectrum of sub-section Ⅱ. **c** 2π-Multi-taper method (MTM) power spectrum of sub-section Ⅰ indicating the eccentricity, obliquity, and precession cycles. (For interpretation of the references to color in this figure legend, the reader is referred to the web version of this article.)

calcite is endothermic and favored at higher temperatures, therefore a higher Mg/Ca ratio could reflect a relative drier climate condition with stronger evaporation (Chamberlain et al., 2013). The chemical index of alternation (CIA, the molar ratio of Al_2O_3 to Al_2O_3 + CaO + Na_2O + K_2O) could also be used as an indicator of paleoclimate: high CIA values indicate a humid climate with a stronger chemical weathering (Fedo et al., 1995; Price and Velbel, 2003). Our geochemical element analyses show that Mg/Ca ratio,

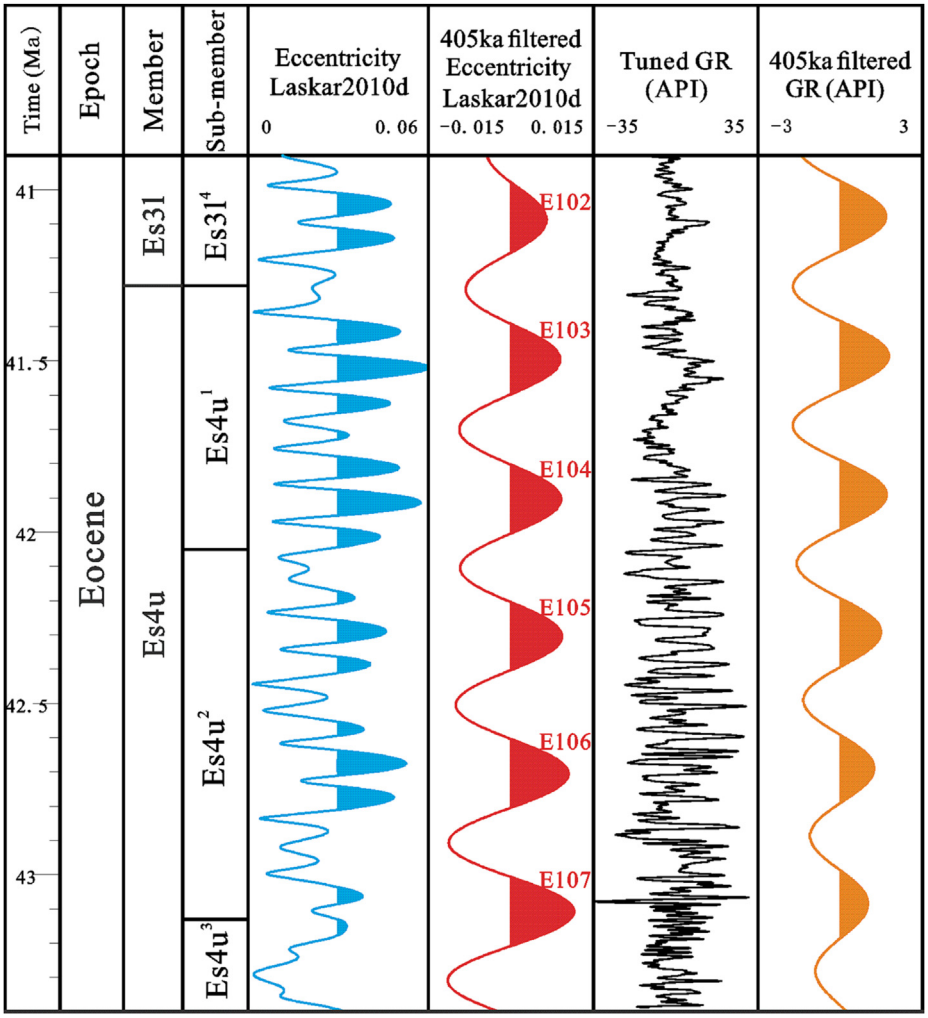

Fig. 6. GR series tuned to the astronomical solution in the time domain using the 405 kyr filter (high eccentricity half cycle indicated).

Na/Al ratio and the chemical index of alternation (CIA, the molar ratio of Al_2O_3 to Al_2O_3 + CaO + Na_2O + K_2O) vary considerably in the vertical direction of the study interval (Fig. 3g, h, j). The Mg/Ca ratio of sub-section Ⅰ is wildly fluctuated ranging from 0.01 to 1 with an average of 0.2, and then decreases to a relatively low value during sub-section Ⅱ with an average of 0.1 (Fig. 3g). The Na/Al ratio has a similar trend as the Mg/Ca ratio: the sub-section Ⅰ has a higher Na/Al ratio (0.09 to 0.55, average: 0.18) than the sub-section Ⅱ (0.09 to 0.13, average: 0.1) (Fig. 3h). The CIA of sub-section Ⅰ can be as low as 40 with an average of 62.6, and rises to a stable high value above 70 during sub-section Ⅱ (Fig. 3j). Thus, from sub-section Ⅰ to sub-section Ⅱ, the samples' Mg/Ca, Na/Al ratios lowered and the CIA increased substantially. These records indicate a humid trend from sub-section Ⅰ to sub-section Ⅱ, although the proxies don't reveal a consistent transition time: the Mg/Ca ratio shows a sharp decline at the boundary of subsection Ⅰ and Ⅱ; the dolomite content shows a gradual decline and the CIA shows a gradual increase around the boundary; the Na/Al ratio is the slowest to change. The reason for this is that different climate proxies have different responding mechanisms and sensitivities to paleoclimate changes. In addition, the dominant lithofacies change from dolomitic shale interbedded with calcareous shale in sub-section Ⅰ to the calcareous shale in sub-section Ⅱ. The sub-section Ⅰ shale has a higher dolomite content, and the cryptocrystalline microscopic characteristics of the dolomite as well as the existence of anhydrite at the bottom of Es4u of the Shahejie Formation in the study area all pointing to a stronger evaporative paleo-environment for the sub-section Ⅰ shale. Besides, Ti content and U/Th ratios could be used to analyze the terrigenous supply and redox conditions of the sedimentary environment respectively (Hatch and Leventhal, 1992; Rimmer, 2004), and the results of our samples show that from sub-section Ⅰ to sub-section Ⅱ terrigenous input increased and reducing condition declined (Fig. 3e, f). Moreover, the sedimentary rates recovered from cyclostratigraphy analysis display a rapid increase from ~6.1 cm/kyr to 9~10 cm/kyr at the boundary of the two sub-sections (Fig. 3n, o). Therefore, based on the combined analysis of petrology, mineral compositions, paleoclimate indicators and sedimentary rates, it is indicated that from the sedimentary period of sub-section Ⅰ to sub-section Ⅱ the paleoclimate experienced an evident humidification in the Dongying depression of the Bohai Bay Basin.

5. Discussion

5.1. Obliquity forcing in the Bohai Bay Basin before 41.9 Ma

The laminated structures of the middle Eocene calcareous shale in the Bohai Bay Basin have been hypothesized to be formed by seasonal climate changes, with duration of each light–dark couplet about one year (Liang et al., 2017; Shi et al., 2021; Zhao et al., 2019). The light carbonate laminae composed of micritic calcite

and dolomite are formed in the spring and summer. Photosynthesis of algae blooms in the warm summer help induce the micritic calcite and when the evaporation is stronger due to high temperature, cryptocrystalline dolomite is precipitated. The dark laminae composed of terrigenous detritus and organic matter are formed in the autumn and winter. When the temperature is lowered in the autumn and winter the micritic calcite vanish and are replaced by terrigenous clastic sediments, and the death of algae provides dark organic matter (Shi et al., 2021).

According to our mineralogy and paleoclimate records in the Dongying Depression, an evident humidification is recognized at ~41.9 Ma, consistent with the timing of the shift from obliquity dominated to eccentricity dominated orbital forcing. The 40 kyr obliquity cycles are filtered for the sub-section Ⅰ shale and combining with our high resolution XRD results as well as TOC analysis it is shown that the high obliquity half cycles have a higher dolomite, clay and TOC content than the low obliquity half cycles (Fig. 7a-c). And phase analyses prove that the dolomite content and TOC are positively correlated with the obliquity signal (Fig. 7d, e). In addition, from the microscopic characteristics of the light–dark lamina couplet, when the obliquity is high, more cryptocrystalline dolomite laminae can be observed and the dark organic rich clay laminae are thicker and contain more organic matter (Fig. 4C, D). When the obliquity is low, the light laminae are mostly composed of micritic calcite and the dark laminae contain less organic matter. All these show that the deposition of sub-section Ⅰ shale is paced by 40 kyr obliquity signal. Obliquity could affect the insolation amount at high latitudes (Hinnov, 2018) and pace the organic carbon burial in middle-high latitudes (Huang et al., 2021). The recording of obliquity signals at low latitudes could be attributed to the remote effect of high latitude ice sheet fluctuations (Bosmans et al., 2015; Kong et al., 2023). Westerhold and Röhl (2009) put forward that the obliquity signal was amplified by the initial ice sheet at high latitudes during the Eocene cooling trend. The sub-section Ⅰ shale was deposited during the Eocene cooling phase, and strong obliquity cycles are recognized in the Bohai Bay Basin both in this study and previous cyclostratigraphy studies (Jin et al., 2022; Shi et al., 2021; Shi et al., 2019). The sudden weakening of obliquity signal in the Shahejie Formation might be due to the occurrence of global warming events following the cooling trend. However, an unresolved question remains: what is the driving mechanism of the obliquity forcing in the Bohai Bay Basin? Obliquity controls the seasonal distribution of solar radiation: when obliquity is high, the subsolar point in boreal summer moves farther north and middle-high latitude areas receive more insolation; when obliquity is low, the subsolar point in boreal summer makes limited movement northward (Hinnov, 2018). Studies show that the longitudinal migration of the Intertropical Convergence Zone (ITCZ) is also paced by obliquity (Liu et al., 2015; Zhang et al., 2022b). ITCZ and the subtropical high north of ITCZ migrate farther north in boreal summer during high obliquity period. Considering that the study area is located at the northernmost part of the arid zone controlled by the subtropical high and close to the humid zone controlled by the westerlies (Fig. 1A), and the lamina deposition characteristics under seasonal variations (Fig. 4), we propose a possible obliquity driving mechanism of the sub-section Ⅰ shale: when the obliquity is high, the subsolar point as well as the location of subtropical high moves more northward in the spring/summer, which results in a more arid spring/summer in the Bohai Bay Basin and deposited carbonate laminae with a higher dolomite content; in the autumn/winter the location of subtropical high moves more southward and the Bohai Bay Basin would experience a more humid autumn/winter with more westerly moisture which contributes to more terrigenous detrital input and more organic matter; while when obliquity is low, the Bohai Bay Basin would experience a decrease in seasonal climate differences. Depositional models of high obliquity period and low obliquity period are illustrated in the Fig. 8. This obliquity dominated

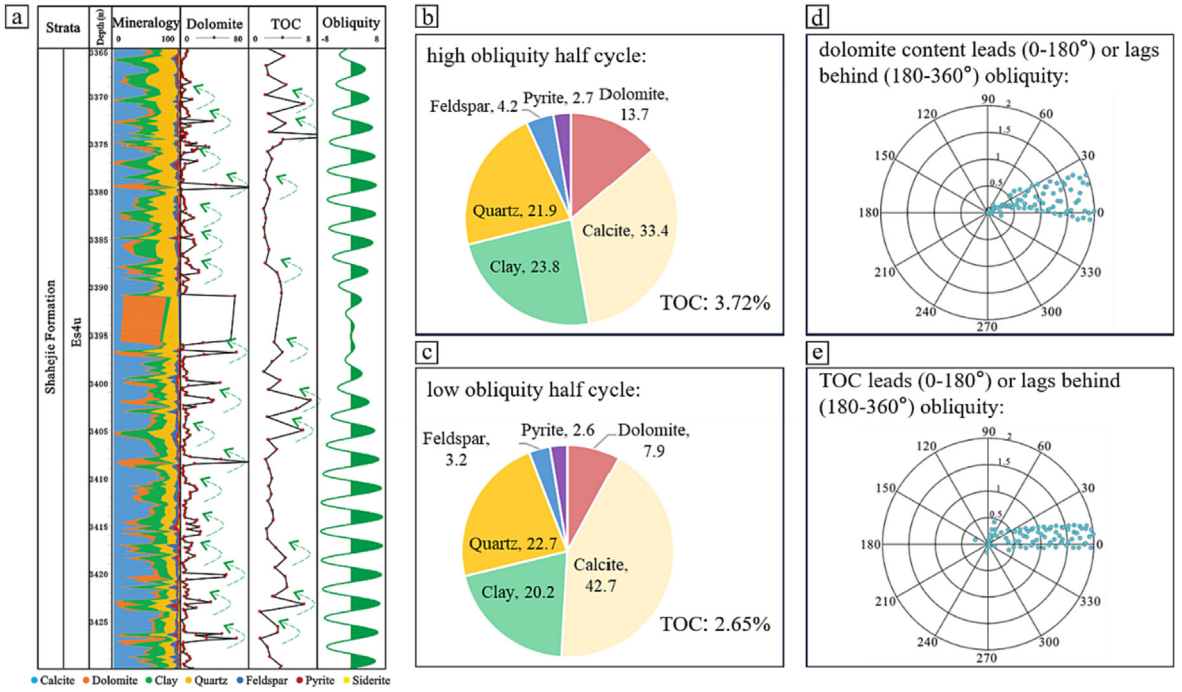

Fig. 7. Obliquity cycles in the sub-section Ⅰ shale. a 40 kyr obliquity signal, mineralogy and TOC content of the sub-section Ⅰ shale (high obliquity half cycle indicated); **b** Component characteristics of high obliquity half cycle; **c** Component characteristics of low obliquity half cycle; **d** Phase polar diagram shows that the dolomite content is positively correlated with obliquity; **e** Phase polar diagram shows that TOC is positively correlated with obliquity.

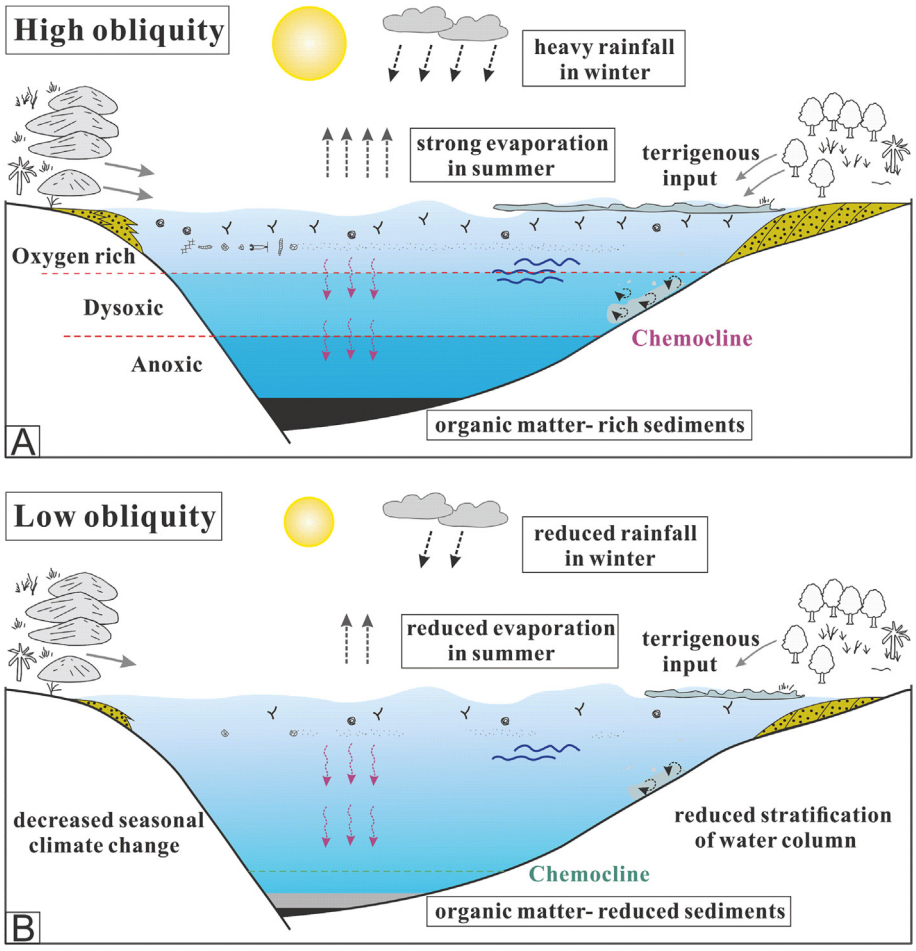

Fig. 8. Depositional models of high obliquity period (A) and low obliquity period (B).

period last about 1.5 Ma from 43.4 Ma to 41.9 Ma, during which time the global temperature was gradually cooling after the Early Eocene Climate Optimum (EECO) (Westerhold et al., 2020).

5.2. Intensification of hydrological cycle linked to global warming

After 41.9 Ma the Dongying Depression of the Bohai Bay Basin experienced an evident humidification and a transition of orbital forcing (Fig. 3). Strong obliquity cycles are replaced by dominant eccentricity cycles as shown in our time series analysis (Fig. 5). The power shift of astronomical cycles in the study area could also be observed from several previous researches, without being paid serious attention to (Shi et al., 2019; Jin et al., 2022; Ma et al., 2023). The shifts in astronomical signals could reflect paleoclimate transitions. One typical example is the mid-Pleistocene transition (MPT): in the high-latitude North Atlantic, the paleoclimate periodicity shifted from obliquity cycles to short eccentricity cycles during the MPT; at the same time in the monsoon-induced middle-latitude East Asia, a dominant precession periodicity was replaced by combined 100, 41, and 23-kyr cycles after the MPT (Pisias and Moore, 1981; Raymo et al., 2006; Sun et al., 2019). For the middle Eocene shale of Bohai Bay Basin, evolutionary fast Fourier transform spectra of GR proxy and magnetic susceptibility proxy at well NY1 and well FY1 all present a power shift from obliquity dominated cycles in the lower part to eccentricity dominated cycles in the upper part (Supplementary Fig. 1).

Our component analysis shows that the high eccentricity half cycles in the sub-section Ⅱ have a more content of terrigenous clastic minerals (quartz, feldspar, clay in total: 50%) than the low eccentricity half cycles (quartz, feldspar, clay in total: 46.4%) and TOC content is also higher in the high eccentricity half cycles (TOC average: 4.18%) than the low eccentricity half cycles (TOC average: 2.31%). Besides, Ma et al. (2019) obtained a series of bulk carbonate $\delta^{18}O$ data of the well NY1 and we identified a good positive correlation between the isotope data and our filtered short eccentricity signal in the sub-section Ⅱ shale. Positive excursions of carbonate $\delta^{18}O$ occur during every eccentricity high as shown in the Fig. 9. The bulk carbonate $\delta^{18}O$ of the well NY1 has a range of 2.9‰ which is too large if the $\delta^{18}O$ variation is caused by the change of lake temperature (Ma et al., 2019; Kim and O'Neil, 1997). Considering the location of the basin in the paleogeography map, the climate of the Bohai Bay Basin was affected by both westerlies and East Asian summer monsoons. Although previous studies indicated that the Paleogene climate in China transitioned from planetary wind dominated pattern to the East Asian monsoon dominated pattern at around 25–22 Ma (Song et al., 1983; Sun and Wang, 2005; Wu et al., 2018), existence of earlier East Asian monsoons is more and more demonstrated (Licht et al., 2014; Quan et al., 2011; Quan et al., 2012). The moisture brought by the westerlies is depleted in heavier $\delta^{18}O$ through long distance transport and as a result has a lower $\delta^{18}O$ value than the vapor brought by the East Asian summer monsoons. Therefore we interpret that the carbonate $\delta^{18}O$ variation is induced by moisture supply change, and the positive excursions which occur at high eccentricity are corresponding to the intensification of the East Asian monsoons (Fig. 10). Then we compared our records with the ocean bottom

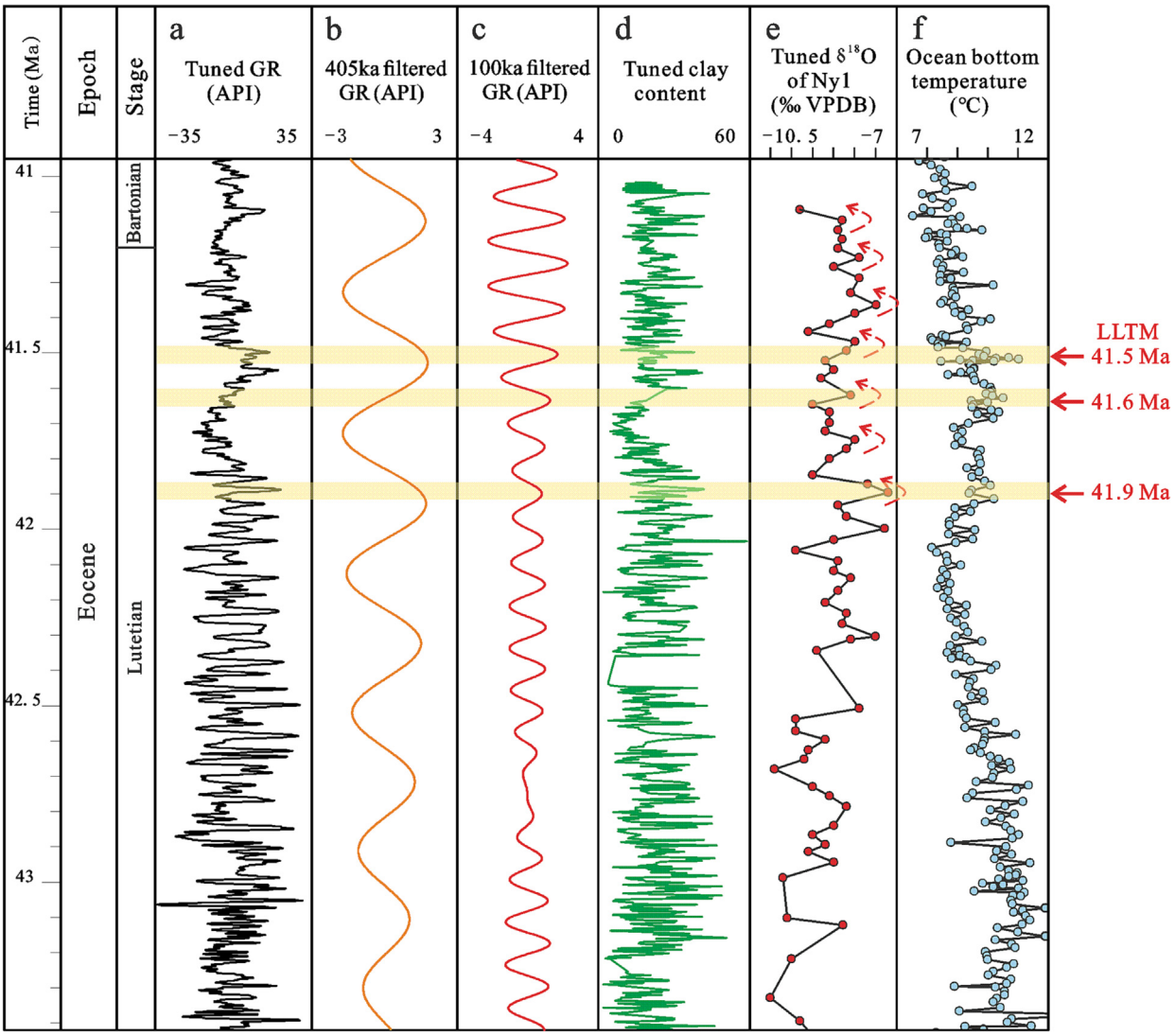

Fig. 9. Linkage between the eccentricity cycles of sub-section Ⅱ shale and global warming events. a GR series of the well NY1 tuned to the time domain; b 405 kyr component filtered from the GR series; c 100 kyr component filtered from the GR series; d clay content of the well NY1 tuned to the time domain; e $\delta^{18}O$ of the well NY1 tuned to the time domain; f ocean bottom temperature calculated from the benthic foraminifera $\delta^{18}O$ at the ODP site 1263 (isotope data from Westerhold et al. (2020)).

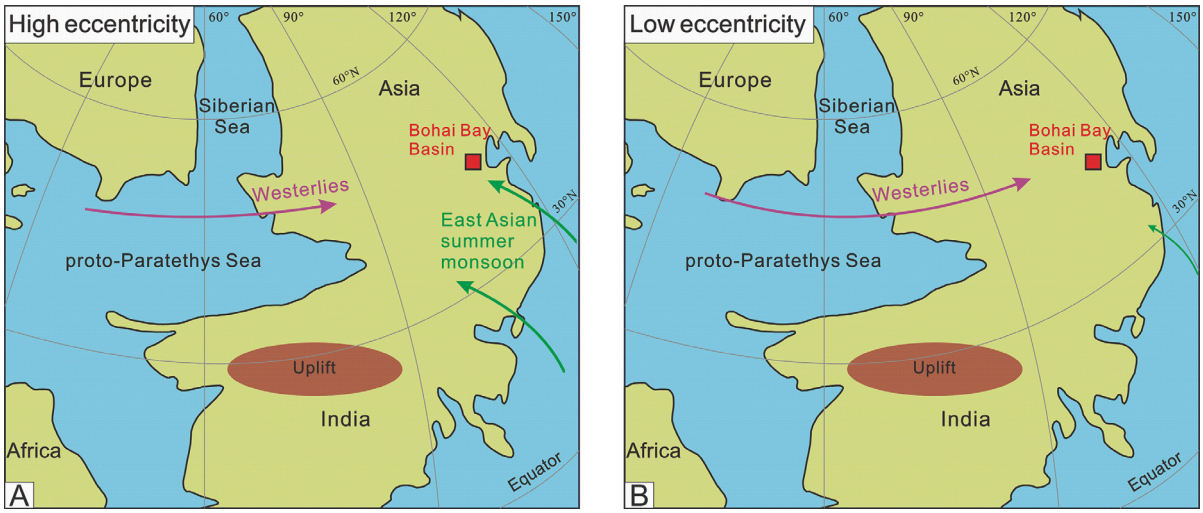

Fig. 10. Demonstrational models of high eccentricity period (A) and low eccentricity period (B) (middle Eocene paleogeography map modified from Bosboom et al. (2014a), Meijer et al. (2019), showing the study site and atmospheric configurations).

temperature calculated from the benthic foraminifera $\delta^{18}O$ at the ODP site 1263 (isotope data from Westerhold et al. (2020)) and revealed a linkage between the terrestrial records of the Bohai Bay Basin and the global climate. As shown in the Fig. 9, three positive excursions of the bulk carbonate $\delta^{18}O$ of the NY1 shale are simultaneous with three global warming events at ~41.5 Ma, 41.6 Ma and 41.9 Ma. Among them the global warming event at ~41.5 Ma is recently defined as the Late Lutetian Thermal Maximum (LLTM, or called the chron C19r event) caused by elevated atmospheric CO_2 concentration (Intxauspe-Zubiaurre et al., 2018; Rivero-Cuesta et al., 2020; Westerhold et al., 2018). From what has been discussed above, from ~41.9 Ma to 41 Ma the global warming events at high eccentricity induced the intensifications of the East Asian summer monsoons at the Bohai Bay Basin, which resulted in more terrigenous detrital input, more organic matter and positive excursions of carbonate $\delta^{18}O$ in the shale deposition of the Shahejie Formation in the Bohai Bay Basin.

6. Conclusions

In summary, our results show an orbital variability shift from obliquity dominated cycles to eccentricity dominated cycles and an evident humidification for the terrestrial climate in East Asia at around 41.9 Ma. Before 41.9 Ma, obliquity played an important role in controlling the position of the subtropical high over East Asia and consequently affected the seasonal climate as well as the deposition of the laminated shale of the Shahejie Formation. After 41.9 Ma the terrestrial climate is paced by eccentricity and eccentricity maxima are related to the global warming events during ~41.9–41.5 Ma including the LLTM hyperthermal event. We accredited the 41.9 Ma terrestrial climate transition in the Bohai Bay Basin to an intensification of the East Asian monsoons probably responding to the elevated atmospheric CO_2 concentration during the concurrent global warming event. The paleoclimate of middle Eocene East Asia reorganized from the planetary wind controlled pattern to the East Asian monsoon dominant pattern. This study could possibly shed a light on establishing more sophisticated climate simulation models of both Eocene and future global warming world.

CRediT authorship contribution statement

Yu Han: Formal analysis, Writing – original draft. **Yingchang Cao:** Supervision, Methodology. **Chao Liang:** Conceptualization, Supervision. **Keyu Liu:** Investigation. **Fang Hao:** Investigation.

Declaration of Competing Interest

The authors declare that they have no known competing financial interests or personal relationships that could have appeared to influence the work reported in this paper.

Acknowledgements

We thank the Shengli Oilfield, Sinopec for providing the core samples and well data. We are grateful for the thoughtful comments and suggestions from the editors and reviewers. This study was supported by the Shandong Provincial Key Research and Development Program, China (2020ZLYS08), the National Natural Science Foundation of China (Nos. 42272119, 41821002), Taishan Scholars Program, China (No. TSQN201812030), and the Fundamental Research Funds for the Central Universities, China (2022CX06001A).

Appendix A. Supplementary data

Supplementary data to this article can be found online at https://doi.org/10.1016/j.gr.2023.08.020.

References

Anagnostou, E., John, E.H., Edgar, K.M., Foster, G.L., Ridgwell, A., Inglis, G.N., Pancost, R.D., Lunt, D.J., Pearson, P.N., 2016. Changing atmospheric CO_2 concentration was the primary driver of early Cenozoic climate. Nature 533, 380–384.
Aswasereelert, W., Meyers, S.R., Carroll, A.R., Peters, S.E., Smith, M.E., Feigl, K.L., 2013. Basin-scale cyclostratigraphy of the Green River Formation, Wyoming. Geol. Soc. Am. Bull. 125, 216–228.
Barrett, P., 2003. Palaeoclimatology: cooling a continent. Nature 421, 221–223.
Bosboom, R.E., Dupont-Nivet, G., Houben, A.J.P., Brinkhuis, H., Villa, G., Mandic, O., Stoica, M., Zachariasse, W.J., Guo, Z.J., Li, C.X., Krijgsman, W., 2011. Late Eocene sea retreat from the Tarim Basin (west China) and concomitant Asian paleoenvironmental change. Paleogeogr. Paleoclimatol. Paleoecol. 299, 385–398.
Bosboom, R.E., Dupont-Nivet, G., Grothe, A., Brinkhuis, H., Villa, G., Mandic, O., Stoica, M., Huang, W., Yang, W., Guo, Z., Krijgsman, W., 2014a. Linking Tarim Basin sea retreat (west China) and Asian aridification in the late Eocene. Basin Res. 26, 621–640.
Bosboom, R.E., Abels, H.A., Hoorn, C., van den Berg, B.C.J., Guo, Z.J., Dupont-Nivet, G., 2014b. Aridification in continental Asia after the Middle Eocene Climatic Optimum (MECO). Earth Planet. Sci. Lett. 389, 34–42.
Bosmans, J.H.C., Hilgen, F.J., Tuenter, E., Lourens, L.J., 2015. Obliquity forcing of low-latitude climate. Clim. Past 11, 1335–1346.
Carrapa, B., DeCelles, P.G., Wang, X., Clementz, M.T., Mancin, N., Stoica, M., Kraatz, B., Meng, J., Abdulov, S., Chen, F.H., 2015. Tectono-climatic implications of Eocene Paratethys regression in the Tajik basin of central Asia. Earth Planet. Sci. Lett. 424, 168–178.
Chamberlain, C.P., Wan, X., Graham, S.A., Carroll, A.R., Doebbert, A.C., Sageman, B.B., Blisniuk, P., Kent-Corson, M.L., Wang, Z., Chengshan, W., 2013. Stable isotopic evidence for climate and basin evolution of the late Cretaceous Songliao basin, China. Paleogeogr. Paleoclimatol. Paleoecol. 385, 106–124.
Chen, D., Pang, X.Q., Wang, Y.W., Dong, Y.X., Jiang, F.J., Li, L., Pang, H., Bai, H., Pang, B., Qin, R., Jiang, H., 2020. Palaeoenvironmental periodisms of middle Eocene terrestrial sediments in Bohai Bay Basin, eastern China, and their implications for organic matter accumulation. Mar. Pet. Geol. 112, 104060.
Dupont-Nivet, G., Hoorn, C., Konert, M., 2008. Tibetan uplift prior to the Eocene-Oligocene climate transition: evidence from pollen analysis of the Xining Basin. Geology 36, 987–990.
Fedo, C.M., Nesbitt, H.W., Young, G.M., 1995. Unraveling the effects of potassium metasomatism in sedimentary rocks and paleosols, with implications for paleoweathering conditions and provenance. Geology 23, 921–924.
Giorgioni, M., Jovane, L., Rego, E.S., Rodelli, D., Frontalini, F., Coccioni, R., Catanzariti, R., Ozcan, E., 2019. Carbon cycle instability and orbital forcing during the Middle Eocene Climatic Optimum. Sci. Rep. 9, 9357.
Greenwood, D.R., Wing, S.L., 1995. Eocene continental climates and latitudinal temperature gradients. Geology 23, 1044–1048.
Guo, Z.T., F., R.W., Z., H.Q., B., W.H., S., Q.Y., X., Z.R., Z., P.S., J., W.J., Y., Y.B., S., L.T., 2002. Onset of Asian desertification by 22 Myr ago inferred from loess deposits in China. Nature 416, 159–163. 10.1038/416159a.
Guo, Z.T., Sun, B., Zhang, Z.S., Peng, S.Z., Xiao, G.Q., Ge, J.Y., Hao, Q.Z., Qiao, Y.S., Liang, M.Y., Liu, J.F., Yin, Q.Z., Wei, J.J., 2008. A major reorganization of Asian climate by the early Miocene. Clim. Past 4, 153–174.
Hatch, J.R., Leventhal, J.S., 1992. Relationship between inferred redox potential of the depositional environment and geochemistry of the Upper Pennsylvanian (Missourian) Stark Shale Member of the Dennis Limestone, Wabaunsee County, Kansas, U.S.A. Chem. Geol. 99, 65–82.
He, J., Ding, W., Jiang, Z., Jiu, K., Li, A., Sun, Y., 2017. Mineralogical and chemical distribution of the Es3L oil shale in the Jiyang Depression, Bohai Bay Basin (E China): implications for paleoenvironmental reconstruction and organic matter accumulation. Mar. Pet. Geol. 81, 196–219.
Hinnov, L.A., 2018. Chapter One - Cyclostratigraphy and Astrochronology in 2018. Academic Press.
Huang, H., Gao, Y., Ma, C., Jones, M.M., Zeeden, C., Ibarra, D.E., Wu, H., Wang, C., 2021. Organic carbon burial is paced by a ~173-ka obliquity cycle in the middle to high latitudes. Sci. Adv. 7, 9489–9498.
Huang, R.D., Jiang, F.J., Chen, D., Qiu, R.Y., Hu, T., Fang, L.H., Hu, M.L., Wu, G.Y., Zhang, C.X., Lv, J.H., Wu, Y.P., Huang, L.L., 2023. Astrochronology and carbon-isotope stratigraphy of the Fengcheng Formation, Junggar Basin: terrestrial evidence for the Carboniferous-Permian Boundary. Gondw. Res. 116, 1–11.
Intxauspe-Zubiaurre, B., Martínez-Braceras, N., Payros, A., Ortiz, S., Dinarès-Turell, J., Flores, J.-A., 2018. The last Eocene hyperthermal (Chron C19r event, ~41.5 Ma): chronological and paleoenvironmental insights from a continental margin (Cape Oyambre, N Spain). Paleogeogr. Paleoclimatol. Paleoecol. 505, 198–216.
Jin, S.D., Liu, S.B., Li, Z., Chen, A.Q., Ma, C., 2022. Astrochronology of a middle Eocene lacustrine sequence and sedimentary noise modeling of lake-level changes in Dongying Depression, Bohai Bay Basin. Paleogeogr. Paleoclimatol. Paleoecol. 585. https://doi.org/10.1016/j.palaeo.2021.110740.
Kim, S.-T., O'Neil, J.R., 1997. Equilibrium and nonequilibrium oxygen isotope effects in synthetic carbonates. Geochim. Cosmochim. Acta 61, 3461–3475.

Kong, X.X., Jiang, Z.X., Cai, Y., 2023. Orbital and sub-orbital pacing of mudstones in the Dongying Depression, eastern China: implications for middle Eocene East Asian climate evolution. Geol. Soc. Am. Bull. https://doi.org/10.1130/B36606.1.
Laskar, J., Fienga, A., Gastineau, M., Manche, H., 2011. La2010: a new orbital solution for the long-term motion of the Earth. Astron. Astrophys. 532. https://doi.org/10.1051/0004-6361/201116836.
Li, M.S., Kump, L.R., Hinnov, L.A., Mann, M.E., 2018. Tracking variable sedimentation rates and astronomical forcing in Phanerozoic paleoclimate proxy series with evolutionary correlation coefficients and hypothesis testing. Earth Planet. Sci. Lett. 501, 165–179.
Li, M.S., Hinnov, L., Kump, L., 2019. Acycle: time-series analysis software for paleoclimate research and education. Comput. Geosci. 127, 12–22.
Liang, C., Jiang, Z.X., Cao, Y.C., Wu, J., Wang, Y.S., Hao, F., 2017. Sedimentary characteristics and origin of lacustrine organic-rich shales in the salinized Eocene Dongying Depression. Geol. Soc. Am. Bull. 130, 154–174.
Licht, A., van Cappelle, M., Abels, H.A., Ladant, J.B., Trabucho-Alexandre, J., France-Lanord, C., Donnadieu, Y., Vandenberghe, J., Rigaudier, T., Lecuyer, C., Terry Jr., D., Adriaens, R., Boura, A., Guo, Z., Soe, A.N., Quade, J., Dupont-Nivet, G., Jaeger, J. J., 2014. Asian monsoons in a late Eocene greenhouse world. Nature 513, 501–506.
Liu, Y., Lo, L., Shi, Z.G., Wei, K.Y., Chou, C.J., Chen, Y.C., Chuang, C.K., Wu, C.C., Mii, H. S., Peng, Z.C., Amakawa, H., Burr, S.G., Lee, S.Y., Delong, L.K., Elderfield, H., Shen, C.C., 2015. Obliquity pacing of the western Pacific Intertropical Convergence Zone over the past 282, 000 years. Nat. Commun. 6, 10018.
Lunt, D.J., Elderfield, H., Pancost, R., Ridgwell, A., Foster, G.L., Haywood, A., Kiehl, J., Sagoo, N., Shields, C., Stone, E.J., Valdes, P., 2013. Warm climates of the past–a lesson for the future? Philos. Trans. R. Soc. A-Math. Phys. Eng. Sci. 371, 20130146. https://doi.org/10.1098/rsta.2013.0146.
Ma, Y.Q., Fan, M.J., Lu, Y.C., Liu, H.M., Zhang, S.P., Liu, X.F., 2019. Stable isotope record of middle Eocene summer monsoon and its instability in eastern China. Glob. Planet. Change 175, 103–112.
Ma, Y.Q., Fan, M.J., Li, M.S., Ogg, J.G., Zhang, C., Feng, J., Zhou, C.H., Liu, X.F., Lu, Y.C., Liu, H.M., Eldrett, J.S., Ma, C., 2023. East Asian lake hydrology modulated by global sea-level variations in the Eocene warmhouse. Earth Planet. Sci. Lett. 602, 117925.
Meijer, N., Dupont-Nivet, G., Abels, H.A., Kaya, M.Y., Licht, A., Xiao, M., Zhang, Y., Roperch, P., Poujol, M., Lai, Z., Guo, Z., 2019. Central Asian moisture modulated by proto-Paratethys Sea incursions since the early Eocene. Earth Planet. Sci. Lett. 510, 73–84.
Meyers, S.R., 2015. The evaluation of eccentricity-related amplitude modulation and bundling in paleoclimate data: an inverse approach for astrochronologic testing and time scale optimization. Paleoceanography 30, 1625–1640.
Meyers, S.R., 2019. Cyclostratigraphy and the problem of astrochronologic testing. Earth-Sci. Rev. 190, 190–223.
Molnar, P., Boos, W.R., Battisti, D.S., 2010. Orographic controls on climate and Paleoclimate of Asia: thermal and mechanical roles for the Tibetan Plateau. Annu. Rev. Earth Planet. Sci. 38, 77–102.
Pisias Jr., N.G., Moore, T.C., 1981. The evolution of the Pleistocene climate: a time series approach. Earth Planet. Sci. Lett. 52, 450–458.
Price, J.R., Velbel, M.A., 2003. Chemical weathering indices applied to weathering profiles developed on heterogeneous felsic metamorphic parent rocks. Chem. Geol. 202, 397–416.
Qiang, X.K., An, Z.S., Song, Y.G., Chang, H., Sun, Y.B., Liu, W.G., Ao, H., Dong, J.B., Fu, C. F., Wu, F., Lu, F.Y., Cai, Y.J., Zhou, W.J., Cao, J.J., Xu, X.W., Ai, L., 2010. New eolian red clay sequence on the western Chinese Loess Plateau linked to onset of Asian desertification about 25 Ma ago. Sci. China-Earth Sci. 54, 136–144.
Quan, C., Liu, Y.S., Utescher, T., 2011. Paleogene evolution of precipitation in Northeastern China supporting the middle Eocene intensification of the East Asian Monsoon. PALAIOS 26, 743–753.
Quan, C., Liu, Y.S., Utescher, T., 2012. Eocene monsoon prevalence over China: a paleobotanical perspective. Paleogeogr. Paleoclimatol. Paleoecol. 365–366, 302–311.
Raymo, M.E., Lisiecki, L.E., Nisancioglu, K.H., 2006. Plio-Pleistocene ice volume, antarctic climate, and the global $\delta^{18}O$ record. Science 313, 5786.
Rimmer, S.M., 2004. Geochemical paleoredox indicators in Devonian-Mississippian black shales, Central Appalachian Basin (USA). Chem. Geol. 206, 373–391.
Rivero-Cuesta, L., Westerhold, T., Alegret, L., 2020. The Late Lutetian Thermal Maximum (middle Eocene): first record of deep-sea benthic foraminiferal response. Paleogeogr. Paleoclimatol. Paleoecol. 545. https://doi.org/10.1016/j.palaeo.2020.109637.
Rohling, E.J., Marino, G., Grant, K.M., 2015. Mediterranean climate and oceanography, and the periodic development of anoxic events (sapropels). Earth Sci. Rev. 143, 62–97.
Sawyer, E.W., 1986. The influence of source rock type, chemical weathering and sorting on the geochemistry of clastic sediments from the Quetico Metasedimentary Belt, Superior Province. Canada. Chem. Geol. 55, 77–95.
Schnyder, J., Ruffell, A., Deconinck, J.F., Baudin, F., 2006. Conjunctive use of spectral gamma-ray logs and clay mineralogy in defining late Jurassic-early Cretaceous palaeoclimate change (Dorset, UK). Palaeogeogr. Palaeoclimatol. Palaeoecol. 229, 303–320.
Scotese, C.R., 2016. Global Climate Change (Modern Times to 540 million years ago), Earth History: The Evolution of the Earth System. Northwestern University, Evanston, IL.
Shi, J.Y., Jin, Z.J., Liu, Q.Y., Zhang, R., Huang, Z.K., 2019. Cyclostratigraphy and astronomical tuning of the middle Eocene terrestrial successions in the Bohai Bay Basin, Eastern China. Glob. Planet. Change. 174, 115–126.
Shi, J., Jin, Z., Liu, Q., Fan, T., Gao, Z., 2021. Sunspot cycles recorded in Eocene lacustrine fine-grained sedimentary rocks in the Bohai Bay Basin, eastern China. Glob. Planet. Change 205. https://doi.org/10.1016/j.gloplacha.2021.103614.
Song, Z.C., Li, W.B., He, C.Q., 1983. Cretaceous and Palaeogene palynofloras and distribution of organic rocks in China. Sci. China Ser. B-Chem. 26, 538–549.
Sun, X.J., Wang, P.X., 2005. How old is the Asian monsoon system?—Palaeobotanical records from China. Palaeogeogr. Palaeoclimatol. Palaeoecol. 222, 181–222.
Sun, Y.B., Yin, Q.Z., Crucifix, M., Clemens, S.C., Araya-Melo, P., Liu, W.G., Qiang, X.K., Liu, Q.S., Zhao, H., Liang, L.J., Chen, H.Y., Li, Y., Zhang, L., Dong, G.C., Li, M., Zhou, W.J., Berger, A., An, Z.S., 2019. Diverse manifestations of the mid-Pleistocene climate transition. Nat. Commun. 10, 352.
Westerhold, T., Marwan, N., Drury, A.J., Liebrand, D., Agnini, C., Anagnostou, E., Barnet, J.S.K., Bohaty, S.M., De Vleeschouwer, D., Florindo, F., Frederichs, T., Hodell, D.A., Holbourn, A.E., Kroon, D., Lauretano, V., Littler, K., Lourens, L.J., Lyle, M., Palike, H., Rohl, U., Tian, J., Wilkens, R.H., Wilson, P.A., Zachos, J.C., 2020. An astronomically dated record of Earth's climate and its predictability over the last 66 million years. Science 369, 1383–1387.
Westerhold, T., Röhl, U., 2009. High resolution cyclostratigraphy of the early Eocene: new insights into the origin of the Cenozoic cooling trend. Clim. Past 5, 309–327.
Westerhold, T., Röhl, U., 2013. Orbital pacing of Eocene climate during the Middle Eocene Climate Optimum and the chron C19r event: missing link found in the tropical western Atlantic. Geochem. Geophys. Geosyst. 14, 4811–4825.
Westerhold, T., Röhl, U., Donner, B., Frederichs, T., Kordesch, W.E.C., Bohaty, S.M., Hodell, D.A., Laskar, J., Zeebe, R.E., 2018. Late Lutetian thermal maximum—crossing a thermal threshold in earth's climate system? Geochem. Geophys. Geosyst. 19, 73–82.
Wu, L.J., Wang, F.K., Wang, D.H., Fu, M., Jia, Y.H., 2018. The lithologic differences between the third and fourth members of the Eocene Shahejie Formation in the Bohai Bay Basin and the associated climatic evolution. Geol. J. 53, 788–802.
Wu, H.C., Zhang, S.H., Hinnov, L.A., Jiang, G.Q., Yang, T.S., Li, H.Y., Wan, X.Q., Wang, C. S., 2014. Cyclostratigraphy and orbital tuning of the terrestrial upper Santonian-Lower Danian in Songliao Basin, northeastern China. Earth Planet. Sci. Lett. 407, 82–95.
Zachos, J.C., Dickens, G.R., Zeebe, R.E., 2008. An early Cenozoic perspective on greenhouse warming and carbon-cycle dynamics. Nature 451, 279–283.
Zachos, J.C., McCarren, H., Murphy, B., Röhl, U., Westerhold, T., 2010. Tempo and scale of late Paleocene and early Eocene carbon isotope cycles: implications for the origin of hyperthermals. Earth Planet. Sci. Lett. 299, 242–249.
Zahid, M.A., Chunmei, D., Lin, C., Gluyas, J., Jones, S., Zhang, X., Munawar, M.J., Ma, C., 2016. Sequence stratigraphy, sedimentary facies and reservoir quality of Es4s, southern slope of Dongying Depression, Bohai Bay Basin, East China. Mar. Pet. Geol. 77, 448–470.
Zhang, Z.S., Flatøy, F., Wang, H.J., Bethke, I., Bentsen, M., Guo, Z.T., 2012. Early Eocene Asian climate dominated by desert and steppe with limited monsoons. J. Asian Earth Sci. 44, 24–35.
Zhang, J.G., Jiang, Z.X., Liang, C., Baars, T.F., Wang, Y.W., Abels, H.A., 2022a. Astronomical forcing of meter-scale organic-rich mudstone-limestone cyclicity in the Eocene Dongying sag, China: implications for shale reservoir exploration. AAPG Bull. 106, 1557–1579.
Zhang, P., Xu, J., Holbourn, A., Kuhnt, W., Xiong, Z.F., Li, T.G., 2022b. Obliquity induced latitudinal migration of the Intertropical Convergence Zone during the past ~410 kyr. Geophys. Res. Lett. 49, e2022GL100039.
Zhao, K., Du, X.B., Lu, Y.C., Xiong, S.P., Wang, Y., 2019. Are light-dark coupled laminae in lacustrine shale seasonally controlled? A case study using astronomical tuning from 42.2 to 45.4 Ma in the Dongying Depression, Bohai Bay Basin, eastern China. Palaeogeogr. Palaeoclimatol. Palaeoecol. 528, 35–49.